

# Impacts of land use change on thermodynamic and dynamic changes of precipitation for the Yangtze River Basin, China

Qian Lin<sup>1,2</sup>  | Jie Chen<sup>1,2</sup>  | Wei Li<sup>1,2</sup> | Kailin Huang<sup>1,2</sup> | Xuezhi Tan<sup>3</sup> | Hua Chen<sup>1,2</sup>

<sup>1</sup>State Key Laboratory of Water Resources and Hydropower Engineering Science, Wuhan University, Wuhan, China

<sup>2</sup>Hubei Key Laboratory of Water System Science for Sponge City Construction, Wuhan University, Wuhan, China

<sup>3</sup>Department of Water Resources and Environment, School of Civil Engineering, Sun Yat-sen University, Guangzhou, China

## Correspondence

Jie Chen, State Key Laboratory of Water Resources and Hydropower Engineering Science, Wuhan University, Wuhan 430072, China.

Email: jiechen@whu.edu.cn

## Funding information

The National Key Research and Development Program of China, Grant/Award Number: 2017YFA0603704; the Hubei Provincial Natural Science Foundation of China, Grant/Award Number: 2020CFA100; the National Natural Science Foundation of China, Grant/Award Number: 52079093; the Overseas Expertise Introduction Project for Discipline Innovation (111 Project), Grant/Award Number: B18037

## Abstract

Many studies found that land use change (LUC) had great impacts on regional precipitation, due to thermodynamic and dynamic responses. However, the relative contributions of these two factors to changes in precipitation due to LUC are rarely investigated. This study quantifies the relative contributions of thermodynamic and dynamic to the changes of mean and extreme precipitation due to LUC based on simulations of the Weather Research and Forecasting (WRF) model. The Yangtze River Basin (YRB) is used as a case study, as it has experienced great LUC during the past decades. Four land use scenarios (two factual cases and two hypothetical reforestation scenarios) were used to test the sensitivity of precipitation changes to LUC. Changes in mean and extreme precipitation over the YRB for all seasons are attributed to thermodynamic and dynamic changes using 500-hPa geopotential height and precipitation data derived from the simulations of WRF. The results show that the factual process of LUC results in a decrease in summer mean daily precipitation and precipitation extremes in most areas of the YRB (except for the middle reaches of the YRB), while the hypothetical reforestation contributes to an increase in summer mean and extreme precipitation, and the impacts of reforestation on increasing precipitation are limited. The thermodynamic change contributes to an increase in seasonal mean daily precipitation, extreme precipitation totals and occurrence frequency of precipitation extremes with contributions ranging from 94 to 102%, which is the main contributor of changes in precipitation due to LUC. The dynamic change only makes a small contribution to the change of precipitation. Because the contributions of thermodynamic can be offset by dynamic changes to changes in precipitation, it could result in minimal changes in precipitation and occurrences of precipitation extremes.

## KEY WORDS

dynamic, land use change, precipitation, thermodynamic, WRF, Yangtze River Basin

## 1 | INTRODUCTION

During the past decades, land use/cover change has been an important theme in the study field of global climate change (Sterling *et al.*, 2013). Especially in the mid-1970s, it was recognized that land use change (LUC) modified the surface albedo, thus changing the energy exchanges of the surface atmosphere (Otterman, 1974; Charney *et al.*, 1975; Sagan *et al.*, 1979). Therefore, LUC inevitably affects the wind velocity, mixing layer depth and thermal structures of the boundary layer and the local atmospheric circulations which are all associated with precipitation (Demuzere *et al.*, 2013; Grawe *et al.*, 2013). Numerous studies have also showed that LUC could affect the ecosystem structure and impact human being by changing the energy and matter flows, biogeochemical cycles, biosphere-atmosphere interactions, surface radioactive forcing, biodiversity and the sustainable utilization of regional or local environmental resources (Gascoigne *et al.*, 2011; Wang *et al.*, 2014; Geneletti, 2013; Liu *et al.*, 2003a; Dewan *et al.*, 2012; Wang *et al.*, 2015). The influence of LUC on precipitation is due to variations in atmospheric dynamic, thermal and chemical component (Zhang *et al.*, 2019). Therefore, precipitation changes can be either thermodynamic or dynamic. The dynamic change in precipitation is due to the change in atmospheric circulation, while the thermodynamic change is due to the change in conditions such as atmospheric moisture fluxes and latent heat fluxes, and the longwave radiation which are unrelated to atmospheric circulation (Seager *et al.*, 2010; Horton *et al.*, 2015). Some previous studies have examined the linkage between the probability of precipitation events to changes in atmospheric circulation (e.g., Cassano *et al.*, 2007; Coumou *et al.*, 2014; Jezequel *et al.*, 2018). For example, Tan *et al.* (2019) identified trends in occurrences of certain synoptic circulation patterns that have contributed to changes in precipitation intensity and occurrences of precipitation extremes over Canada, and found that most changes in mean and extreme precipitation over Canada were caused by thermodynamic changes.

The Yangtze River Basin (YRB) is one of the most populated regions in the world. During the past decades, lots of human activities, such as reforestation through the Returning Farmland to Forest Program (RFFP), urbanization and damming have taken place in the YRB, resulting in large LUC which have shown significant impacts on climate for this river basin (e.g., Wu *et al.*, 2006; Wang and Zhong, 2014; Li *et al.*, 2017; Kong *et al.*, 2018). However, the relative contribution of changes in atmospheric, thermodynamic and dynamic conditions to changes in precipitation due to LUC is not clear.

Previous studies have identified some primary synoptic circulation patterns contributing to surface weather conditions for the YRB. For example, Southwest China Vortex is an important circulation system that triggers continuous heavy rainfall in the upper reaches of the YRB (Huang *et al.*, 2012). The El Niño Southern Oscillation (ENSO) circulation across the tropical Pacific Ocean is an important cause of atmospheric circulation anomalies in the Northern Hemisphere. During the negative phase of El Niño, the cause of more precipitation amount in the YRB mostly due to the occurrence of anomalous anticyclone circulation in the tropical northwest Pacific (Wang and Yan, 2011). The atmospheric blocking high in the Eurasia mid-high latitudes plays a significant role in summer precipitation over the mid-lower reaches of the YRB, particularly in the Meiyu period (Zhang and Tao, 1998). In addition, the northwest Pacific anticyclone circulation sustains the Meiyu front in the YRB for a long time, and strengthens the pressure gradient to northwest of the southeast coast of China and thus the Meiyu front system (Chang *et al.*, 2000). In addition, Shu *et al.* (2020) identified six predominant synoptic weather patterns using the self-organizing map (SOM) method over the Yangtze River Delta in summer. However, the change in frequency of synoptic patterns has not been linked to the change in precipitation due to LUC, especially for precipitation extremes.

The objectives of this study are (1) to evaluate the impacts of LUC on mean daily precipitation, seasonal extreme precipitation totals and occurrences of extreme precipitation events for the YRB through identifying synoptic circulation patterns using the SOM method and (2) to quantitatively link the effects of LUC on mean daily precipitation, seasonal extreme precipitation totals and occurrences of extreme precipitation events to thermodynamic and dynamic changes. The study area and data are introduced in Section 2 and Section 3 provides a detailed description of the methodology used in this study. Changes in precipitation due to LUC and the relative contribution of changes in thermodynamic and dynamic conditions to changes in precipitation due to LUC are described in Section 4, followed by summary and conclusions in Section 5.

## 2 | STUDY AREA AND DATA

### 2.1 | Study area

The Yangtze River is the longest river in China with its length of about 6,300 km, which originates from the Tanggula Mountains located in Tibet Plateau (Cui *et al.*, 2017). There are nearly 440 million people live in the YRB, which accounts for one third of China's

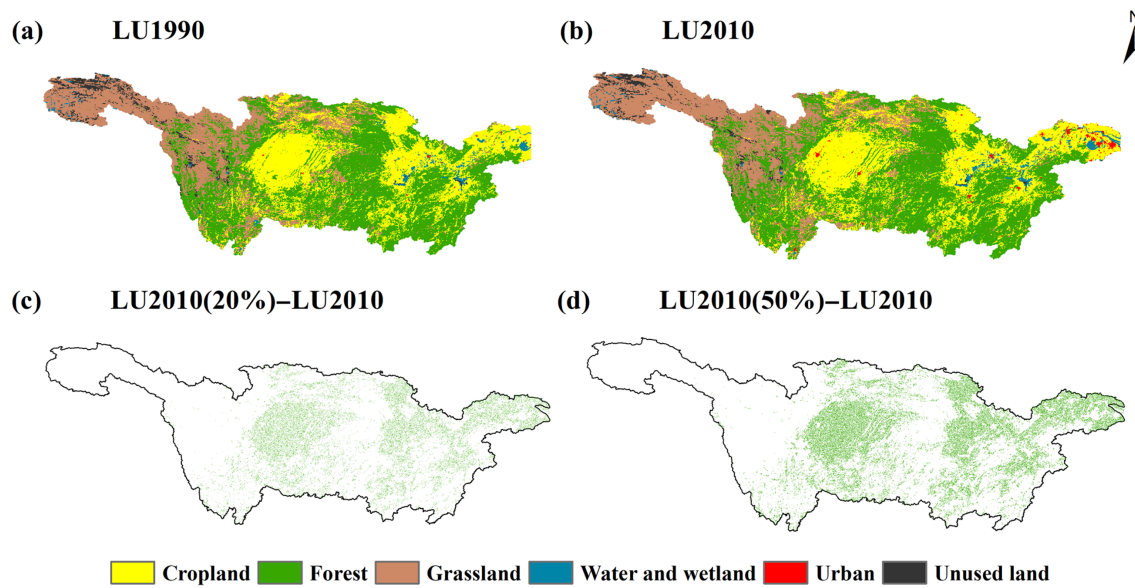


**FIGURE 1** Spatial distribution of the land use of four land use scenarios of the YRB [Colour figure can be viewed at [wileyonlinelibrary.com](http://wileyonlinelibrary.com)]

population (Sang *et al.*, 2013). The economy of the YRB contributes 41.1% of China's gross domestic product (Xu and Ma, 2009). During the past decades, there had been great LUC in the YRB, including urbanization, reforestation, construction of hydraulic engineering facilities and so on, which has great impacts on regional and local climate (e.g., Wu *et al.*, 2006; Wang and Zhong, 2014; Li *et al.*, 2017; Kong *et al.*, 2018). The YRB ( $90^{\circ}33\text{--}122^{\circ}25'\text{E}$ ,  $24^{\circ}30\text{--}35^{\circ}45'\text{N}$ ; Figure 1) is located in the monsoonal climate zone with the mean annual temperature is about  $18^{\circ}\text{C}$  (Zhang *et al.*, 2020). Mean annual precipitation is about 1,067 mm, and most precipitation occurs in summer (June–August), accounting for 70–80% of its annual total precipitation (Yu *et al.*, 2009). In addition, the spatial distribution of mean annual precipitation in the YRB is very uneven, with 270–500 mm in the northwest and 1,600–1,900 mm in the southeast (Yu *et al.*, 2009; Guo *et al.*, 2013). The major paths for moisture transport to the YRB are from the Bay of Bengal (southwest), the South China Sea (south), or the Western Pacific (southeast), depending on time (Wei *et al.*, 2012). In general, the YRB is dominated by the Siberian northwest monsoon in winter; while in summer, the mid-lower reaches are mainly under the control of the East Asia monsoon, and the upper reaches is influenced by the Indian southwest monsoon (Su *et al.*, 2006; Zhao *et al.*, 2009).

## 2.2 | Data

As presented in previous studies (e.g., Huang *et al.*, 2015; Zhi and Ji, 2018), 500-hPa is an important level in the

East Asian monsoon system closely related to the daily weather forecast, and its major modal changes lead to large-scale climate anomalies. Therefore, the 500-hPa geopotential height (GPH) data from 2001 to 2010 derived from the simulation of the WRF model was used in this study to identify the atmospheric circulation pattern. In addition, the sea level pressure data was also used to confirm the results obtained from the 500-hPa GPH, which was derived from the simulation of the WRF model. The daily GPH field at 500-hPa was provided by the European Centre for Medium-Range Weather Forecasts Interim (ERA-Interim) reanalysis data (Dee *et al.*, 2011) at the 24 hr temporal resolution. The observed daily precipitation data obtained from the surface observation stations provided by the China Meteorological Data Sharing Service System, National Meteorological Information Center, China Meteorological Administration (<http://cdc.cma.gov.cn/home.do>). Both the daily 500-hPa GPH data and observed daily average precipitation were interpolated to a spatial resolution of 15 km using the inverse-distance weighting (IDW) method, which were respectively employed to validate the numerical simulations of 500-hPa GPH and precipitation.

In addition, the 1990 and 2010 land use data of the YRB were derived from the Landsat thematic mapper (TM) digital images, which were interpreted based on the geometric shape, texture features, spatial distribution of the ground objects and the spectral characteristics in the images. The spatial resolution of the original land use data was 1 km. The land use categories used in the WRF were the U.S. Geological Survey (USGS) land cover

categories, while the land use categories of the original land use data were defined by Liu *et al.* (2003b). Therefore, the type conversions were performed according to the rules defined by Hu *et al.* (2015).

### 3 | METHODOLOGY

#### 3.1 | Experimental design of LUC

In this study, numerical simulations were used to investigate the influence of LUC in the YRB, which were conducted using version 3.9 of the WRF Advanced Research Core (WRF-ARW) (Skamarock *et al.*, 2008). The WRF model is an atmosphere modelling system developed by NCAR (National Center for Atmospheric Research, USA), NOAA (National Oceanic and Atmospheric Administration, USA) and NCEP (National Centers for Environmental Prediction, USA) and others, which has been designated as a common framework for numerical weather predictions and simulations of regional climate (Zhang *et al.*, 2009; Zhang *et al.*, 2019).

Considering the implementation of the RFFP in the YRB since 1999, and dramatic LUC had happened in the YRB from 1990 to 2010, four different land use scenarios (two factual cases and two hypothetical reforestation scenarios) were used to study the impacts of LUC on regional precipitation: the observed land use in 1990 (LU1990) and 2010 (LU2010); 20% (LU2010 [20%]) and 50% (LU2010 [50%]) of cropland randomly converted into forest on the basis of LU2010 (Figure 1). The LU1990 and LU2010 were used to estimate the impacts of the

observed LUC on precipitation while the other two hypothetical scenarios were used for sensitivity analysis, which can be considered as two extreme cases in the progress of RFFP for the future. As the original land use data in the YRB has been re-classed following the USGS land cover categories, there are two main types of cropland, that is, dry cropland and pasture (code 2), and irrigated cropland and pasture (code 3), and three main types of forest, that is, shrubland (code 8), savanna (code 10) and deciduous broadleaf forest (code 11). When croplands were changed to forests, the proportions of each type of cropland (forest) occupied in the total cropland (forest) were fixed.

Figure 2 shows the double-nested model domains with horizontal grid points of  $81 \times 95$  (spatial resolution of 75 km, d01) and  $161 \times 236$  (spatial resolution of 15 km, d02) used in this study. The vertical structure of the model includes 32 layers covering the whole troposphere. The Lambert conformal map projection was used for the horizontal model coordinates. The WRF model was forced with 0.5° ERA-Interim reanalysis data set. The simulation period was from 2000 to 2010, with the first year taken as spin-up time. To keep the model efficient, the output interval of the outer domain is 7-day, while that of the inner domain is 24-hour. In this study, simulations of precipitation and 500-hPa GPH were both taken from the inner domain (d02).

According to previous studies (e.g., Yin *et al.*, 2014; Huang and Gao, 2017; Gui *et al.*, 2014) and test results (Li *et al.*, 2021, unpublished paper), the most suitable physics schemes used in WRF of this study were identified. Accordingly, the physics schemes used in the WRF

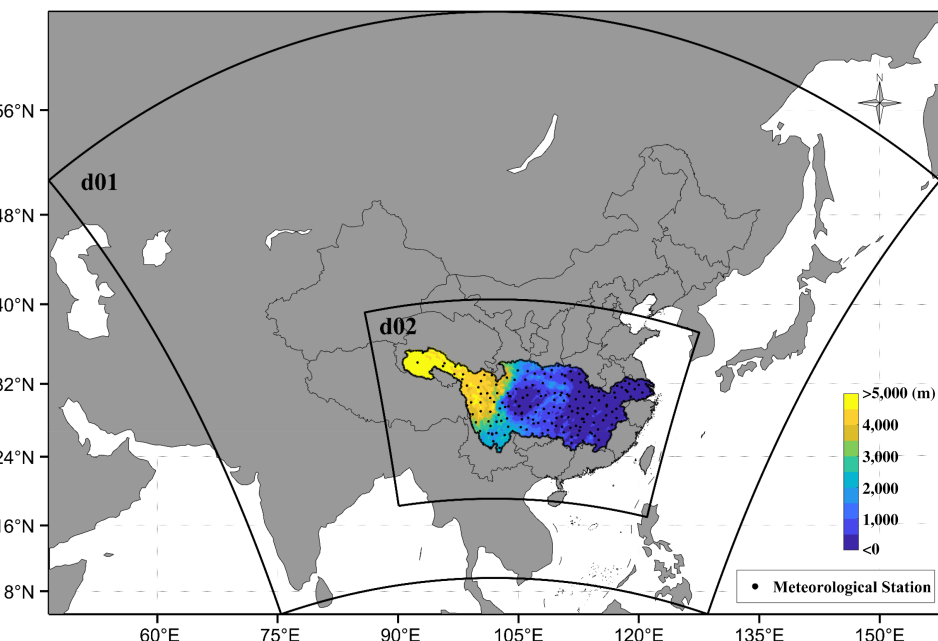


**FIGURE 2** The WRF model domains, locations of the YRB and meteorological stations, and the topography of the YRB [Colour figure can be viewed at [wileyonlinelibrary.com](http://wileyonlinelibrary.com)]

model mainly include the Purdue Lin scheme for microphysical scheme (Lin *et al.*, 1983), the Grell-Devenyi ensemble scheme for cumulus parameterization (Grell and Devenyi, 2002), the Yonsei University PBL scheme for planetary boundary (Hong *et al.*, 2006) and the Noah-MP scheme for the land surface model (Niu *et al.*, 2011; Yang *et al.*, 2011).

Two statistical metrics were used to evaluate the performance of WRF in simulating precipitation/500-hPa GPH: correlation coefficient (*CC*) and mean error (*ME*). They are defined as follows:

$$CC = \frac{\sum((O_i - \bar{O})(S_i - \bar{S}))}{\sqrt{\sum(O_i - \bar{O})^2} \sqrt{\sum(S_i - \bar{S})^2}} \quad (1)$$

$$ME = \frac{\sum(S_i - O_i)}{N} \quad (2)$$

where  $S_i$  and  $O_i$  are simulated and observed precipitation/500-hPa GPH, respectively; and  $N$  is the time period. Statistical significance of *CC* and *ME* was tested by using the paired Student's *t*-test which takes the serial correlation into account (Zwiers and von Storch, 1995) at a significance level of 5%. Given the small sample size for the significance test of precipitation extreme, the bootstrap method (Efron and Tibshirani, 1993) was used to test the statistical significance of precipitation extreme. If only very few grid cells can reach the significance level, a field significance test will be carried out to identify whether statistical significance detected by *t*-test occur by chance for any grid cell. The method of false discovery rate (FDR; Wilks, 2006) was used to test the field significance of the *t*-test.

### 3.2 | Self-organizing map

In order to identify dominant synoptic atmospheric circulation patterns over the YRB for different land use scenarios, the SOM method was used in this study. The SOM method is an unsupervised learning algorithm, which is described as a non-linear mapping of high-dimensional input data onto a topologically ordered array (Kohonen, 1998). Atmosphere modes are continuous, non-linear and span different time scales and space, while the traditional cluster analysis divides most of the data into several classes with the rest as outliers. Compared with the traditional method (e.g., PCA), an advantage of using the SOM method to extract synoptic circulation patterns is that the SOM treats the data as a continuum (Michaelides *et al.*, 2001). In addition, the SOM method could visualize relationships between the different synoptic circulation patterns and the related surface climate (Hewitson and Crane, 2002; Reusch, 2010). Therefore, the

SOM method has been widely used in climate research studies (e.g., Reusch *et al.*, 2005; Cassano *et al.*, 2006a; 2006b; Horton *et al.*, 2015; Tan *et al.*, 2019). A thorough review of the use of the SOM method in atmospheric and oceanic sciences can be found in Liu and Weisberg (2011).

In this study, the analysis of regional precipitation and atmospheric circulation patterns was divided into four seasons, that is, winter (December–February), spring (March–May), summer (June–August) and fall (September–November). The SOM algorithm was trained by daily anomaly GPH field at 500-hPa for all four LUC scenarios. Thus, the atmospheric circulation patterns are represented by spatial variations of 500-hPa geopotential height values which are calculated by subtracting the mean areal geopotential height values (mean GPH values of all grids in the region) from the geopotential height fields. According to pattern similarity, each daily GPH field was assigned to one of the assumed SOM nodes. The final clusters of SOM large-scale circulation patterns are obtained by minimizing the Euclidean distance between iteratively updated nodes and their matching daily GPH field. Therefore, each SOM pattern can be viewed as a representative composite of a number of relatively similar daily large-scale circulation conditions. More details of the SOM method for identifying or extracting synoptic circulation patterns have been described in the literature (e.g., Cassano *et al.*, 2006a, 2006b, 2007; Skific *et al.*, 2009; Reusch, 2010).

Since the SOM method requires allocating the number of nodes for training the data, seven SOM configurations (3–9 nodes) to classify the simulated daily GPH fields were tested to analyse the sensitivity of pattern similarity to the number of SOM nodes for four seasons. The results show that four SOM nodes may not capture subtle features of circulation patterns, but they are sufficient to depict distinct circulations associated with regional precipitation (Figure S1). In addition, studies on temperature extremes (Lee and Feldstein, 2013; Horton *et al.*, 2015) indicated that four nodes were enough in number to capture a diversity of highly generalized circulation patterns, and it can prevent overly similar SOM large-scale circulation patterns.

Once the 4-node SOM GPH patterns were derived, each daily GPH field was assigned to one of the four GPH patterns assumed to have occurred once. Therefore, the grid daily precipitation and extreme precipitation (the top 5% of daily precipitation of each season) were linked to the GPH pattern assigned for that day. Thus, the seasonal mean daily precipitation and extreme precipitation of each GPH pattern for each grid cell can be estimated.

In this study, the statistical significance of differences in node frequency between three land use scenarios and LU2010 was calculated by generating a binomial

distribution following Cassano *et al.* (2007), testing the hypothesis that the difference of the node frequency between the two land use scenarios is zero. If the value of the test statistic exceeds 1.96, the null hypothesis will be rejected at the 95% confidence level and deems the node frequency difference between the two land use scenarios to be significant. The test statistic for testing changes in this frequency assumes two random, independent, binomial processes and is defined as follows:

$$\frac{(p_1 - p_2)}{\sqrt{\frac{p_1(1-p_1)}{n_1}} + \sqrt{\frac{p_2(1-p_2)}{n_2}}}$$

where  $p_1(1 - p_1)/n_1$  and  $p_2(1 - p_2)/n_2$  are estimators of the node frequency variance,  $p_1$  and  $p_2$  are the frequency of occurrence of each pattern in each land use scenario, and  $n_1$  and  $n_2$  are the number of samples over different land use scenarios (for more details see Cassano *et al.*, 2007). Because this statistical test does not account for the effects of serial correlation in the daily 500-hPa GPH fields, and thus likely overestimates the degrees of freedom, so the effective degrees of freedom are approximated by dividing  $n_1$  and  $n_2$  by 5 (Mioduszewski *et al.*, 2016). This indicates that the atmosphere tends to remain in a similar circulation regime for about 5 days, which is estimated empirically from the autocorrelation of this time series of interest. This procedure decreases the degrees of freedom, thus raising the threshold to achieve statistical significance.

### 3.3 | Relative contribution of the thermodynamic and dynamic changes

In order to determine the relative contribution of the thermodynamic and dynamic processes to changes in seasonal mean and extreme precipitation due to LUC, the approach of Cassano *et al.* (2007) was used to assess thermodynamic and dynamic contributions to changes in precipitation of each grid cell. This method is widely used to partition changes in regional surface climate to thermodynamic and dynamics changes because of its simplicity (e.g., Mioduszewski *et al.*, 2016; Tan *et al.*, 2019). Following Cassano *et al.* (2007),

$$P = \sum_{i=1}^N (f_i + \Delta f_i)(p_i + \Delta p_i) \quad (3)$$

$$E = \sum_{i=1}^N (f_i + \Delta f_i)(e_i + \Delta e_i) \quad (4)$$

where  $P$  and  $E$  are the mean daily precipitation or extreme precipitation totals and occurrence frequency of precipitation extremes, respectively;  $p_i$  and  $e_i$  are mean daily precipitation or extreme precipitation totals and the occurrences of precipitation extremes when the  $i$ th SOM circulation pattern occurs, respectively;  $f_i$  is the occurrence frequency of the  $i$ th SOM circulation pattern;  $\Delta f_i$  is the changes in node frequency between two land use scenarios;  $\Delta p_i$  and  $\Delta e_i$  are the changes in node averaged daily net precipitation and occurrences of extreme precipitation events between two land use scenarios, respectively; and  $N$  is the total number of SOM circulation patterns.

$$\Delta P = \sum_{i=1}^N (f_i \Delta p_i + \Delta f_i p_i + \Delta f_i \Delta p_i) \quad (5)$$

$$\Delta E = \sum_{i=1}^N (f_i \Delta e_i + \Delta f_i e_i + \Delta f_i \Delta e_i) \quad (6)$$

In this study, the LU2010 was used as a reference to calculate the changes of mean and extreme precipitation due to LUC. In addition, the total change of seasonal mean daily precipitation, extreme precipitation totals and occurrences of extreme precipitation events (the left-hand sides of Equations (5) and (6)) were divided into three components shown by terms in the right-hand side from left to right: thermodynamic, dynamic and combined contributions for changes related to the  $i$ th SOM circulation pattern. The contribution of thermodynamic change is calculated based on the assumption that the occurrence frequency of SOM circulation pattern keeps constant, and the changes in precipitation are due to the changes in thermodynamic conditions such as atmospheric moisture content, which is described as the first term of Equations (5) and (6). In contrast, the second term of Equations (5) and (6), that is, the dynamic change component is calculated based on the assumption that the precipitation is invariant under the SOM circulation pattern, and the changes in precipitation result from the changes in SOM circulation pattern frequency. The combined contribution which is the final term of Equations (5) and (6) is related to changes in the occurrence frequency of SOM circulation pattern and precipitation.

## 4 | RESULTS AND DISCUSSION

### 4.1 | Performance of WRF in simulating 500-hPa GPH and precipitation

Considering that LU2010 is close to the actual land coverage in the study period, it is used to evaluate the

performance of WRF in simulating 500-hPa GPH and precipitation. Statistical comparisons between the observations and model simulation of 500-hPa GPH and precipitation were firstly conducted using CC and ME as criteria. The CC and ME of mean daily precipitation were calculated using days of each season over 10 years samples (e.g., 92 days/season  $\times$  10 years = 920 samples in summer), while those of extreme precipitation were calculated using the top 5% of the daily precipitation for each season (the sample size is 5% of mean daily precipitation). The first row of Figures 3–5 show the spatial distribution of simulated 500-hPa fields, mean daily precipitation and seasonal extreme precipitation totals. The second and third rows of Figures 3–5 display the results of model validation in terms of CC and ME, respectively.

WRF simulates the 500-hPa GPH fields of the inner domain well for different seasons with CC ranging between 0.4 and 1, and ME less than 50 gpm. For all four seasons, the 500-hPa GPH is significantly overestimated nearly in the whole inner domain at the 5% significance level. While WRF cannot well reproduce the daily precipitation amount with CC belows 0.5 and ME ranges between -6 and 6 mm. Similarly, the seasonal extreme precipitation totals are also not well simulated by WRF.

Although the simulation of seasonal extreme precipitation totals with higher CC than mean daily precipitation, it is not statistically significant for most areas of the YRB. Figures 4 and 5 also show that daily precipitation and extreme precipitation are both significantly underestimated in the lower reaches of the YRB, especially for the rainy season, while the seasonal extreme precipitation totals are overestimated in the upper reaches of the YRB for all seasons and the overestimation is statistically significant at the 5% significance level for spring and summer. Similar results have been found in other studies when using the WRF model. For example, Yu *et al.* (2011) compared the simulated summer monsoon precipitation over China by three different convection schemes in WRF and found the summer precipitation largely underestimated in the lower reaches of the YRB. Huang and Gao (2017) also showed that the simulated precipitation presented a low correlation coefficient in the rainy seasons for most areas of the YRB.

Overall, there is a general consistency between the simulations and observations in the YRB region in which the WRF model can reproduce the 500-hPa GPH during the study period. However, the simulated precipitation presents a large bias, especially for the lower reach of the YRB in the

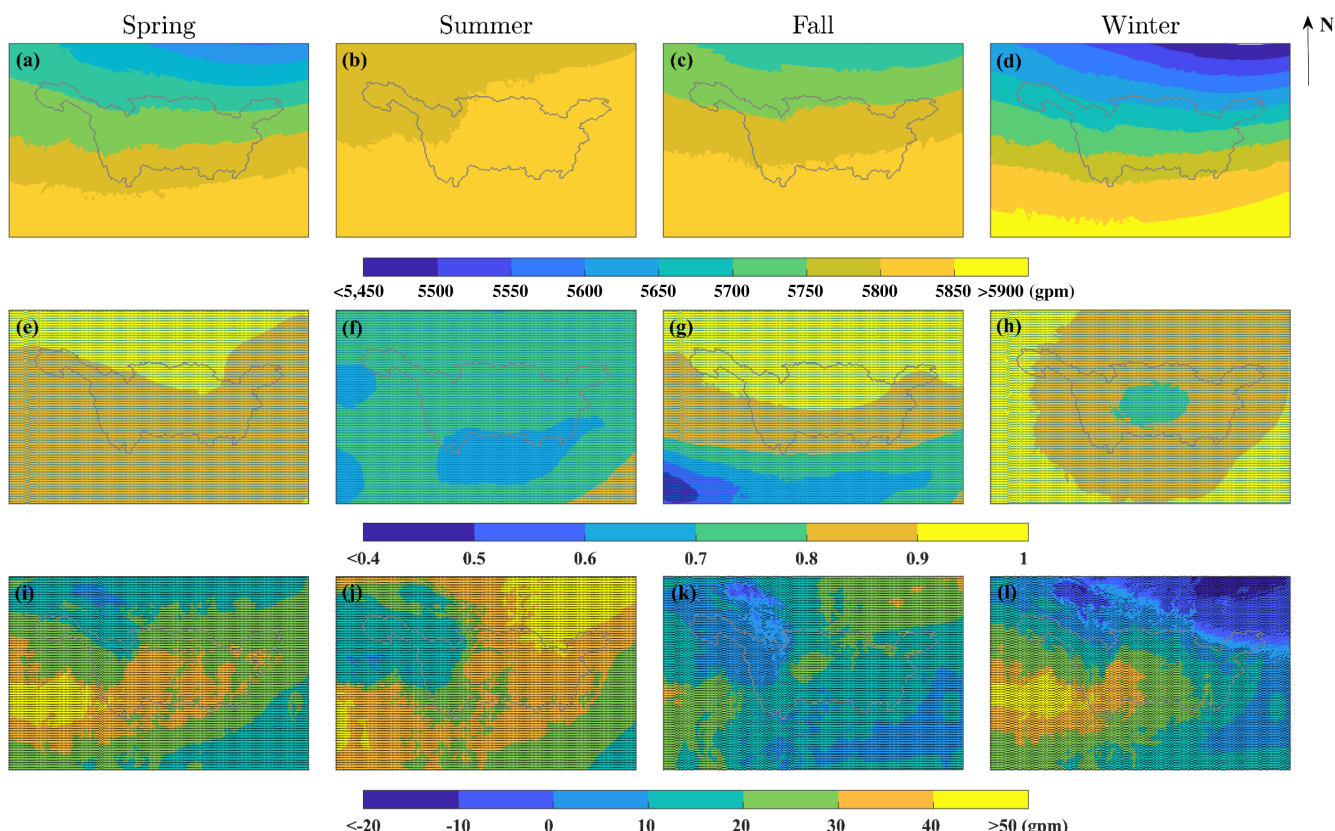


**FIGURE 3** Spatial distribution of simulated 500-hPa GPH fields (a–d), correlation coefficients (e–h) and mean error (i–l) of 500-hPa GPH fields between simulations and observations of LU2010. The stippled regions show statistical significance of correlation coefficient and mean error at the 5% significance level [Colour figure can be viewed at [wileyonlinelibrary.com](http://wileyonlinelibrary.com)]

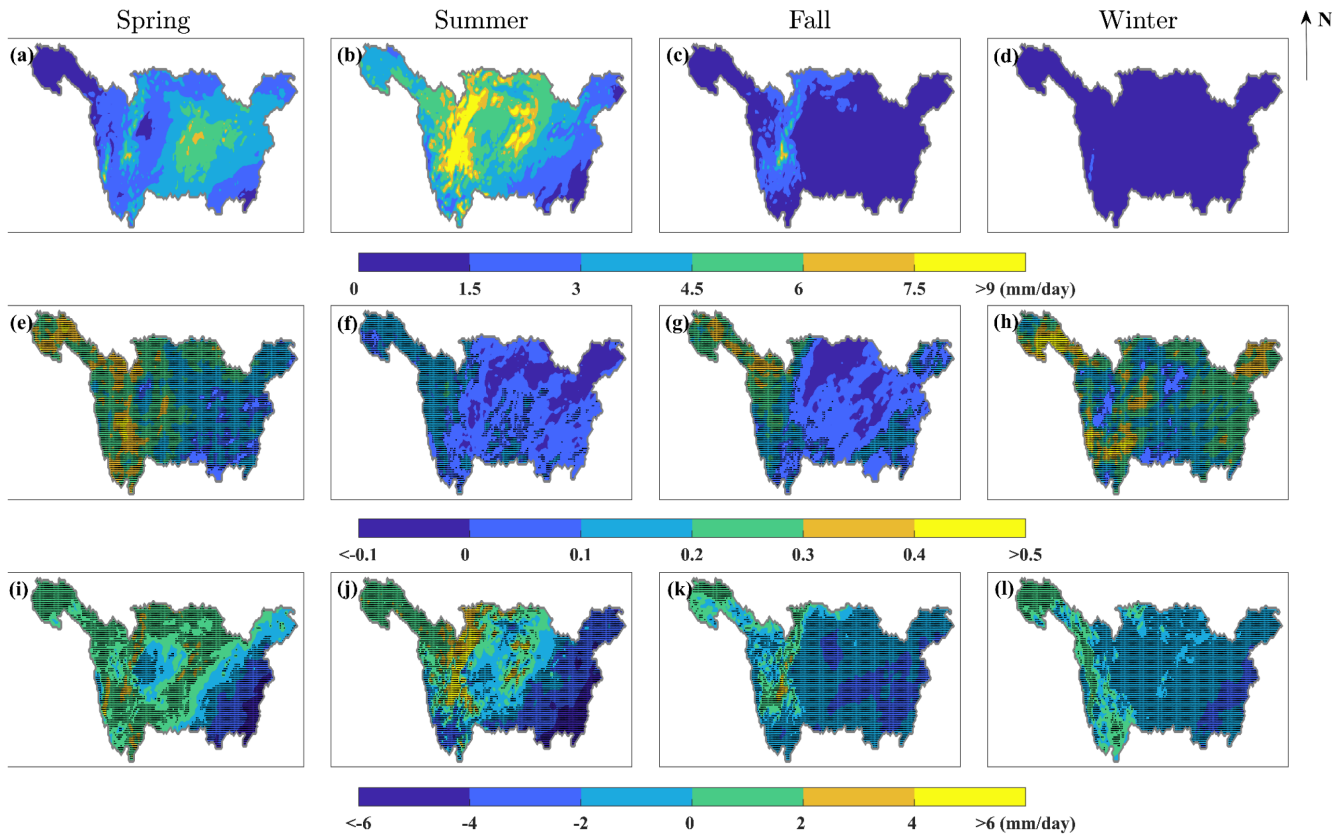


**FIGURE 4** As in Figure 3, but for mean daily precipitation [Colour figure can be viewed at [wileyonlinelibrary.com](http://wileyonlinelibrary.com)]

rainy season. Significant topographic effects generated by upslope motions within the northward moving Indian Ocean storm systems at the southern slope of the Himalayas generally contribute to WRF produce enhanced precipitation (Yu *et al.*, 2011). Besides, only a few stations are available in the upper reaches of the YRB due to the harsh environment and complex terrain, which may lead to observed precipitation be underestimated. The reasons mentioned above may result in underestimation of precipitation in the lower reaches of the YRB and overestimation of precipitation in the upper reaches of the YRB. Meanwhile, the initial meteorological and boundary conditions of the WRF model may be one of the other sources of simulation biases. In addition, the discrepancies between the initial spatial resolution of the WRF and observed data might also contribute to the simulated biases. The detailed evaluation of WRF in simulating climate variables has been presented in Li *et al.* (2021, unpublished paper).

#### 4.2 | Changes in precipitation due to LUC

Even though biases exist in WRF-simulated precipitation, it can still be used to investigate the sensitivity of

precipitation change to LUC, because WRF is driven using the same schemes with only difference in land coverage (e.g., Zhang *et al.*, 2010; Huang and Gao, 2017). Thus, the difference in precipitation among four scenarios can be considered as results of LUC. Figure 6 displays the four major synoptic mid-atmospheric circulation patterns of each season identified by the SOM method. Except for Patterns 1 and 2 in summer, synoptic circulations all show the circulation trend from south to north or from southwest to northeast which origin from the continued strength of the Western Pacific Subtropical High. In addition, 500 hPa GPH fields of certain patterns (i.e., Patterns 1 and 2) in summer show the circulation trend from east to west associated with the Southwest China Vortex, which is an important precipitation system of the upper reaches of the YRB (Chen *et al.*, 2019).

The frequency of each SOM circulation pattern is shown in Table 1 for all four seasons, which shows that there are no obvious differences in the frequency of different circulation patterns. Meanwhile, compared the frequency of each SOM circulation pattern of LU1990 and two hypothetical scenarios with LU2010, differences of frequency for each circulation pattern are not significant at the significance level of 5% (Table S1). Different frequency of each synoptic circulation pattern for different

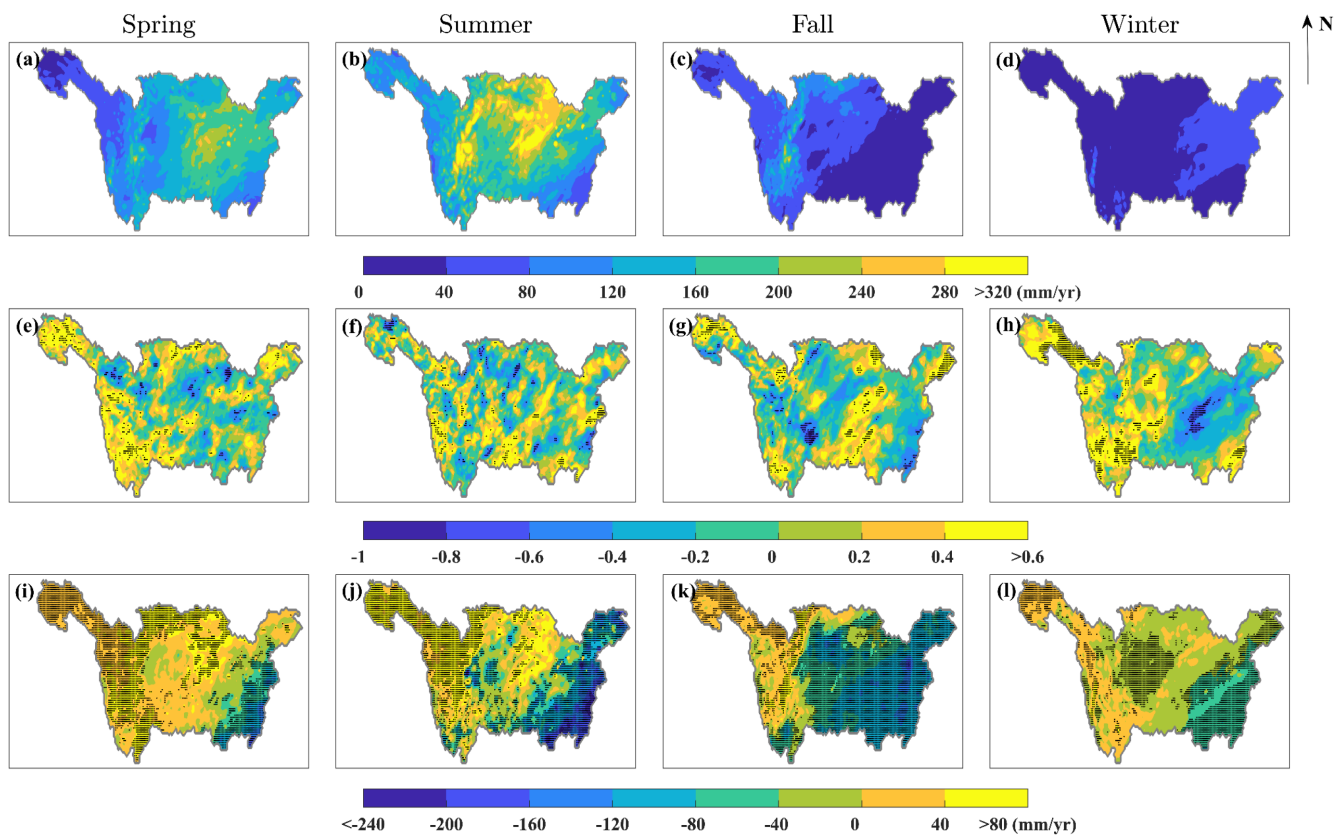


**FIGURE 5** As in Figure 3, but for seasonal extreme precipitation totals [Colour figure can be viewed at [wileyonlinelibrary.com](http://wileyonlinelibrary.com)]

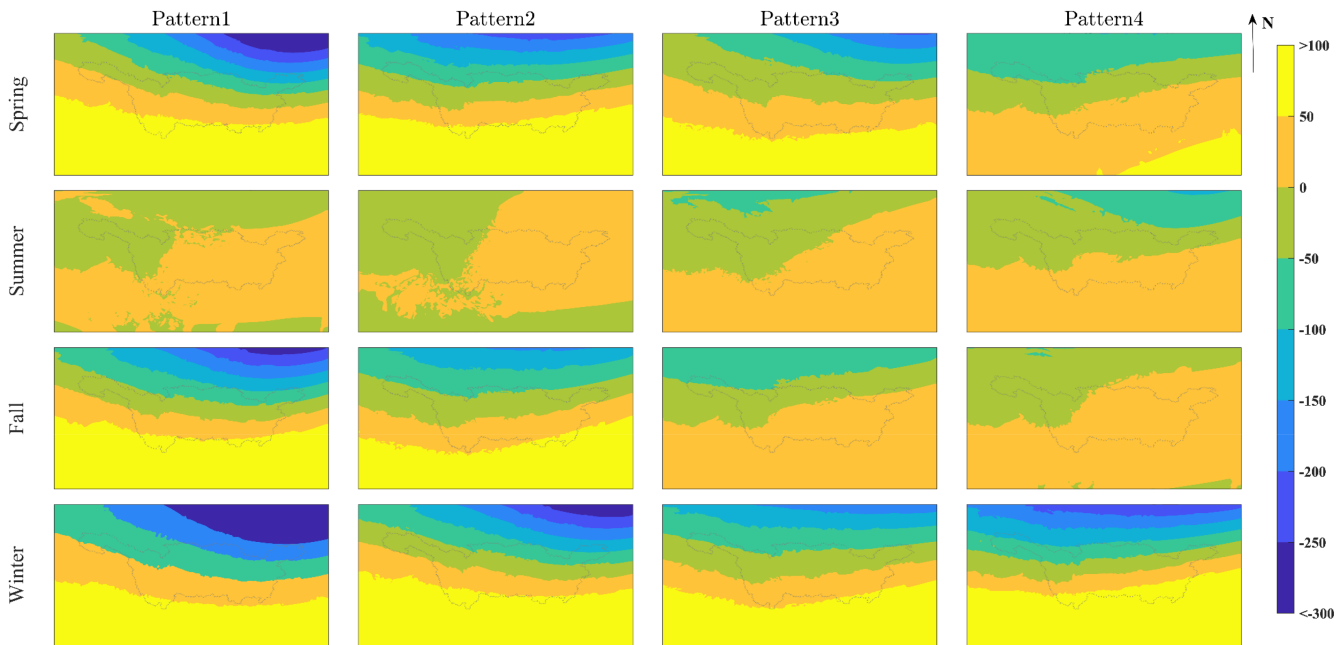


**FIGURE 6** SOM nodes of mid-atmospheric circulation patterns over the YRB for four seasons (unit: Gpm) [Colour figure can be viewed at [wileyonlinelibrary.com](http://wileyonlinelibrary.com)]

land use scenarios contributes to dynamic changes that result in precipitation changes. Thus, it indicates that contributions of dynamic changes are not significant. In

addition, given that, precipitation is mainly concentrated in summer over the YRB, only figures derived from partition analyses of summer are shown.

**TABLE 1** Frequency of SOM circulation patterns derived from the simulated 500-hPa GPH data of LU2010 and differences between LU2010 and LU1990, LU2010(20%) and LU2010(50%) in four seasons (unit: %)

Season	Spring				Summer				Fall				Winter			
	Pattern	P1	P2	P3	P4	P1	P2	P3	P4	P1	P2	P3	P4	P1	P2	P3
LU1990-LU2010	-0.11	0.22	-0.11	0.00	1.85	-3.04	0.76	0.43	-0.11	0.22	0.00	-0.11	0.11	-0.33	0.22	0.00
LU2010	16.20	20.43	29.46	33.91	23.59	26.96	26.52	22.93	16.48	25.06	29.12	29.34	13.97	30.93	20.18	34.92
LU2010(20%)-LU2010	-0.22	0.33	-0.33	0.22	-0.22	-1.63	1.96	-0.11	0.11	0.33	-0.77	0.33	0.11	-0.44	0.22	0.11
LU2010(50%)-LU2010	-0.22	0.22	-0.22	0.22	0.00	1.52	-0.65	-0.87	-0.11	0.44	-0.22	-0.11	0.11	-0.55	0.33	0.11

In order to better analyse the impacts of LUC on precipitation, the simulated mean daily precipitation, extreme precipitation totals and occurrences of extreme precipitation events of LU2010 is used as a baseline and subtracted by each of the three other scenarios (i.e., LU1990, LU2010 (20%) and LU2010 (50%)) (Figures 7–9).

Comparing the summer mean daily precipitation of LU2010 (20%) and LU2010 (50%) with that of LU2010, it can be seen that reforestation contributes to an increase in summer mean daily precipitation in the YRB, although the effect is limited (Figure 7). In addition, the most obvious LUC between LU1990 and LU2010 is urbanization, thus it can be inferred that mean daily precipitation tends to decrease because of urbanization by comparing LU1990 with LU2010. Although changes of summer mean daily precipitation in some grid cells can reach the significant level, they are not statistically significant when using the FDR test. Figures 8 and 9 show that LUC contributes to a decrease in extreme precipitation totals and occurrences of precipitation extremes in most areas of the YRB by comparing LU1990 with LU2010. However, LUC tends to increase the extreme precipitation in the middle reaches of the YRB. Meanwhile, reforestation increases extreme precipitation totals and the occurrence frequency of precipitation extremes for most study areas, but it decreases extreme precipitation in the middle reaches of the YRB by comparing LU2010(50%) with LU2010. Accordingly, it also indicates that the impacts of reforestation on enhancing extreme precipitation are limited in some study areas (e.g., in the middle reaches of the YRB). In addition, differences in the occurrence frequency of precipitation extremes due to LUC and reforestation are more statistically significant than those in extreme precipitation totals, especially for the upper reaches of the YRB. Generally, the spatial distribution of changes in extreme precipitation totals and occurrences of extreme precipitation events due to LUC are quite consistent, which means that higher occurrences of extreme precipitation events contribute to higher extreme precipitation totals.

The West Pacific Subtropical High (WPSH) is a major component of the East Asian monsoon system, which gives moisture to the YRB and has a great impact on precipitation in summer (Yang and Sun, 2005). Patterns 3 and 4 in summer have circulation trends from south to north, which is associated with WPSH and results in high precipitation in the middle reaches of the YRB. The northwestern Pacific Subtropical High plays a significant role in linking ENSO and precipitation extremes in the YRB. Meanwhile, systems in the mid- and high- latitudes also play an important role in affecting extreme precipitation (Wang and Yan, 2011). Therefore, four circulation

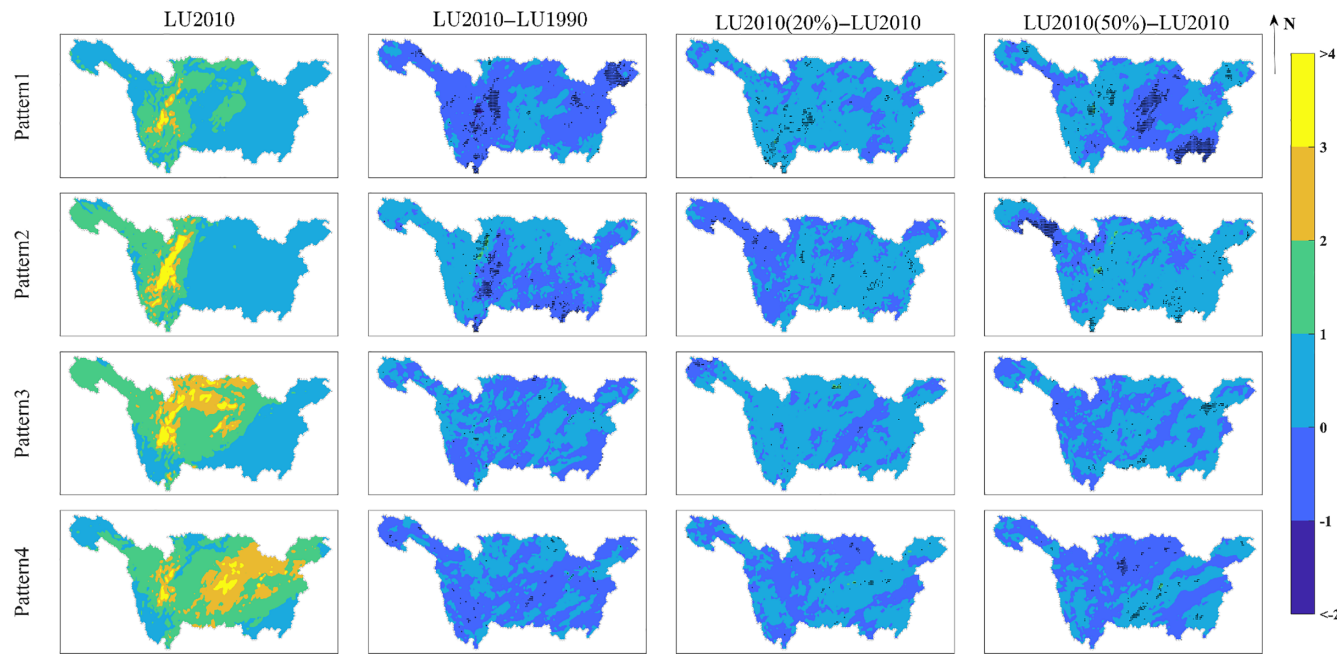


**FIGURE 7** Spatial distribution of mean daily precipitation of LU2010 and differences between LU2010 and LU1990, LU2010 (20%) and LU2010 (50%) in summer (unit: mm/day). The stippled regions show statistically significant changes at the 5% significance level [Colour figure can be viewed at [wileyonlinelibrary.com](http://wileyonlinelibrary.com)]

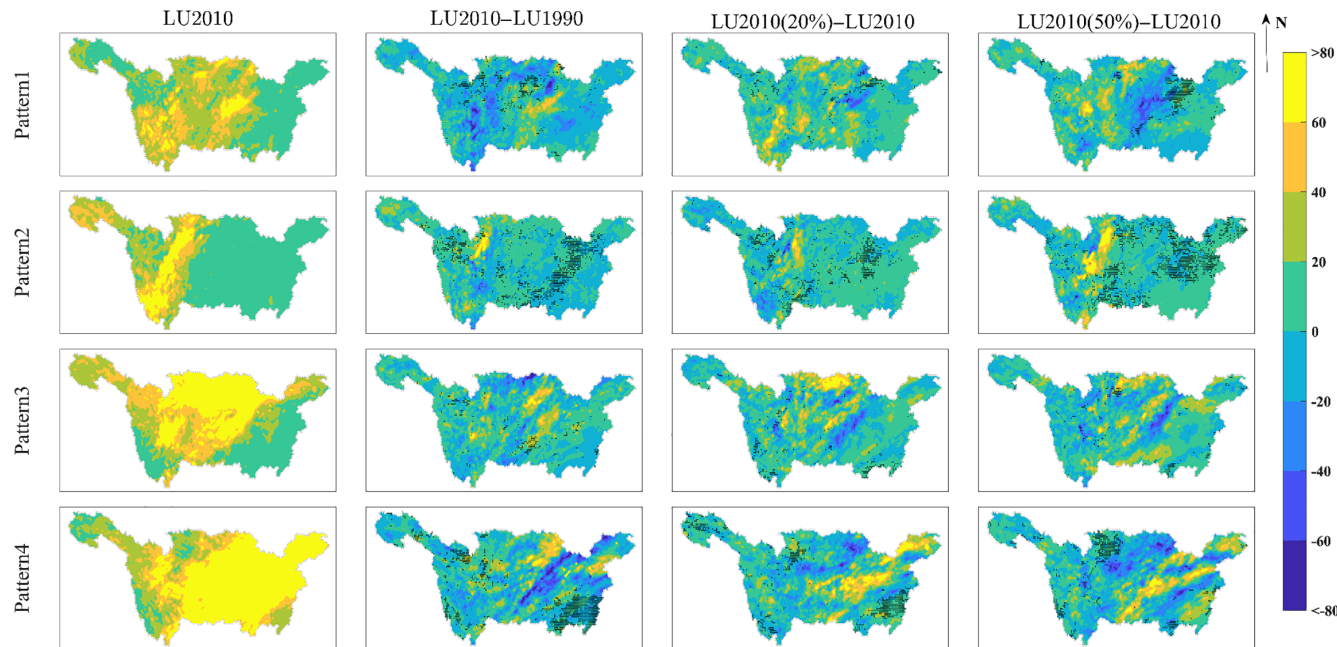


**FIGURE 8** As in Figure 7, but for extreme precipitation totals (unit: mm/yr) [Colour figure can be viewed at [wileyonlinelibrary.com](http://wileyonlinelibrary.com)]

patterns may be all related to synoptic circulation patterns mentioned above, especially Pattern 4 relates to high precipitation for the whole YRB. In addition, the combination of water vapour transport of tropical southwest and mid-latitude northeast may contribute to the increase of precipitation extremes (Wang and Yan, 2011). Circulation patterns derived from the SOM method may

not capture all features of atmospheric circulation patterns mentioned above, which is because of the limited SOM nodes. However, the 500-hPa GPH field is one of the most important components in the East Asian monsoon system, and it can capture the main atmospheric circulation patterns. If precipitation changes of other atmospheric circulation patterns need to be investigated,

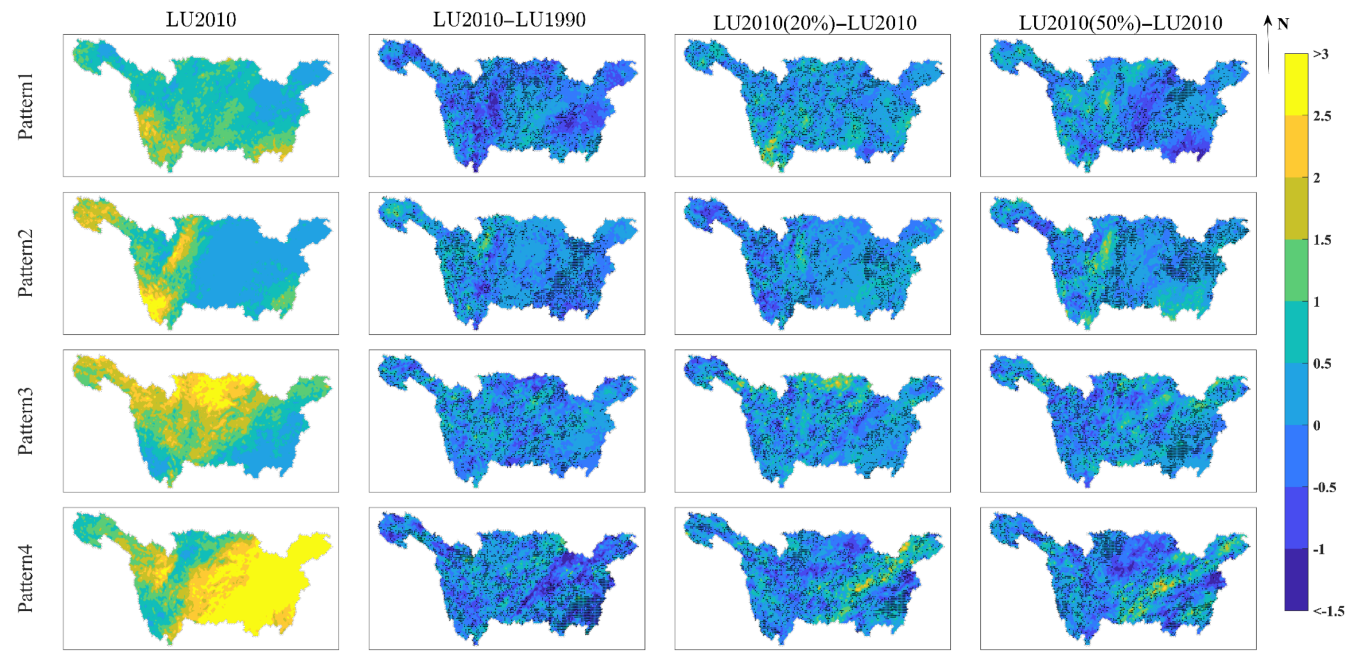


**FIGURE 9** As in Figure 7, but for the occurrence frequency of extreme precipitation events (unit: %) [Colour figure can be viewed at [wileyonlinelibrary.com](http://wileyonlinelibrary.com)]

other variables may be used to identify the circulation pattern.

According to previous studies (e.g., Otterman, 1974; Charney and Stone, Charney *et al.*, 1975; Sagan *et al.*, 1979), it is acknowledged that the LUC process alters the radiation and energy fluxes/balance, and further changes precipitation variations by bio-geophysical effects. Although reforestation tends to increase the mean daily precipitation, its enhancing effect is limited when the reforestation proportion comes to a certain value. It may because the increased precipitation from reforestation is offset by enhanced evapotranspiration (Li *et al.*, 2018). In addition, the results also show that the precipitation frequency can be altered by LUC (Liu and Liu, 2018), which may due to the regulation of regional hydrological cycle (Fu *et al.*, 2017; Li *et al.*, 2018).

#### 4.3 | Thermodynamic and dynamic contributions to precipitation changes

Because of the high spatial variability of precipitation response to changes in thermodynamic and dynamic conditions, some complementary contribution could be offset when thermodynamic and dynamic contributions are in opposition to each other (Tan *et al.*, 2019), so it is useful to investigate relative contributions of thermodynamic and dynamic changes to precipitation changes resulting from LUC. The results displayed in Figure 10 are regional mean values of thermodynamic, dynamic and combined contributions to precipitation changes due to LUC.

By partitioning changes of precipitation over the YRB for all seasons, it is shown that thermodynamic changes contribute to most changes (94–102%) in seasonal mean daily precipitation, seasonal extreme precipitation totals and occurrence frequency of extreme precipitation events due to LUC (Figure 10). For all seasons, thermodynamic changes contribute to the increase in seasonal mean daily precipitation, seasonal precipitation extremes totals, and the occurrences of precipitation extremes. The results also reveal that dynamic changes over some seasons and land use scenarios contribute to a decrease in regional mean daily precipitation and precipitation extremes, such as the 2% decrease in spring mean daily precipitation over LU2010 (20%) and the 2.6% decrease in winter mean daily precipitation over LU2010 (50%), but the contribution of increasing precipitation is minors. Yet, dynamic changes contribute to an increase in mean daily precipitation and occurrences of precipitation extremes for some land use scenarios. For example, the occurrences of precipitation extremes increase 4% in summer over LU1990 compared to LU2010, and spring mean daily precipitation increases 5.7% over LU2010 (50%). In addition, the combined changes of thermodynamic and dynamic show a slight contribution to changes in mean daily, seasonal extreme precipitation totals and occurrence frequency of precipitation extremes with its contribution ranging from –2.3 to 3.3%.

Changes in precipitation of three scenarios are almost (~100%) due to thermodynamic changes for all four seasons. The changes in seasonal precipitation are almost all

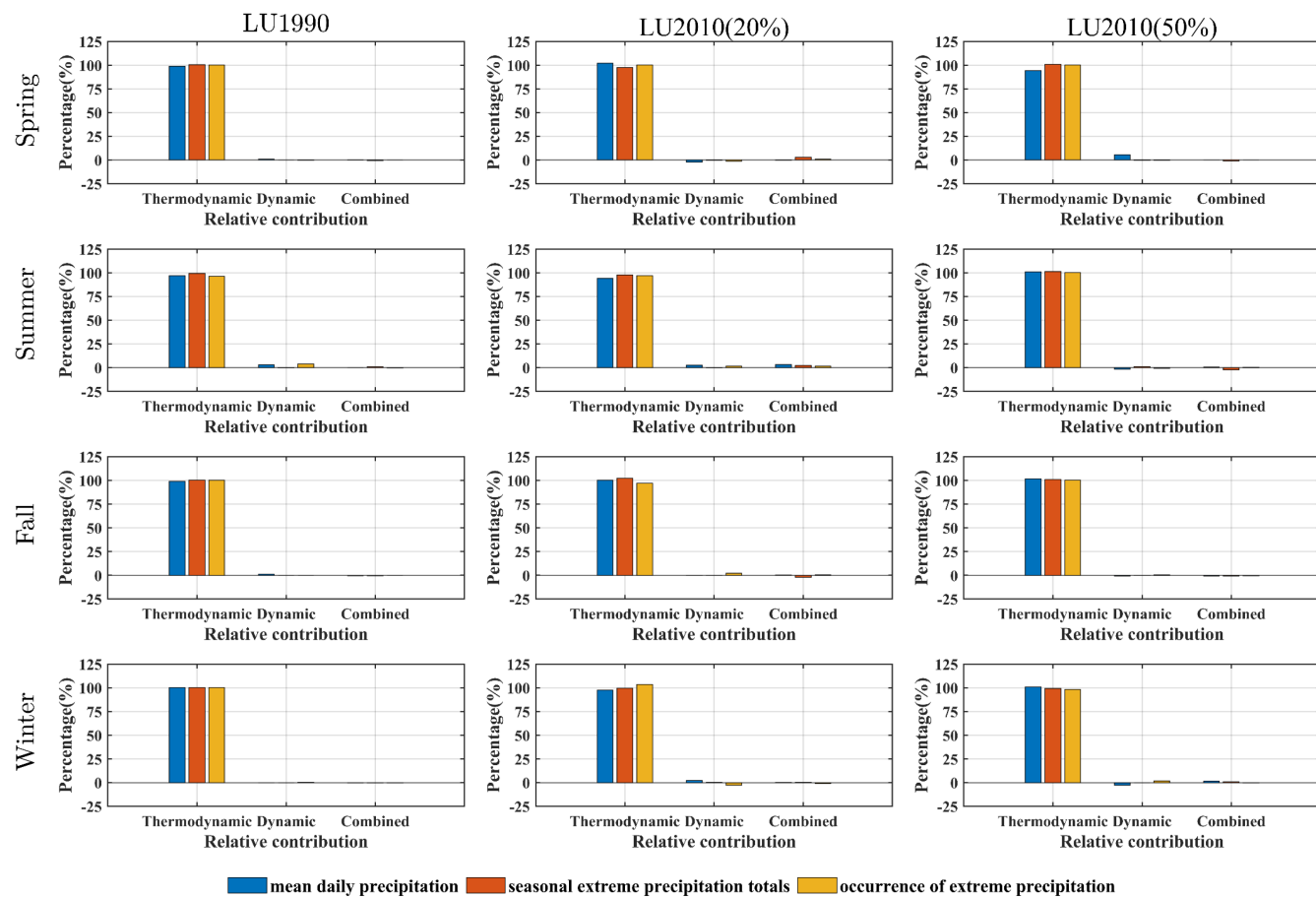


**FIGURE 10** Percentage of changes in the mean daily precipitation, seasonal extreme precipitation totals and occurrence of extreme precipitation events partitioned to thermodynamic, dynamic or dynamic change acting on thermodynamic change (combined) for the YRB and the four seasons [Colour figure can be viewed at [wileyonlinelibrary.com](http://wileyonlinelibrary.com)]

due to positive thermodynamic changes in three scenarios for all seasons, which is partly related to the increased atmospheric moisture due to reforestation. In addition, thermodynamic changes account for a high positive percentage in all seasons over four land use scenarios, but negative dynamic or combined contributions offset thermodynamic contributions which would result in minimal changes in precipitation.

In order to further confirm the results of thermodynamic and dynamic contribution to the changes in precipitation due to LUC, another atmospheric variable, that is, sea level pressure was also used to separate the thermodynamic and dynamic changes in precipitation. The results displayed in Figure S2 show that the thermodynamic change remains the main contributor to precipitation changes due to LUC, which accounts for nearly 100% of the contribution to precipitation changes. In other words, the relative contributions of thermodynamic and dynamic are very similar to those identified by using 500-hPa GPH.

The dynamic change is due to the change in atmospheric motion, while the thermodynamic change is due

to the change in atmospheric moisture content (Emori and Brown, 2005). According to the results, changes in thermodynamic are the main contributor of changes in precipitation due to LUC, which is consistent with the descriptions of Horton *et al.* (2015) and Seager *et al.* (2010). Therefore, the results show that reforestation affects the atmospheric moisture content and generates more precipitation. Because of the negative and positive contributions of thermodynamic and dynamic changes, changes in mean daily precipitation and precipitation extremes over the YRB would be more varied. In general, this study shows that the LUC has a great impact on thermodynamic variables.

## 5 | SUMMARY AND CONCLUSIONS

This study applies the SOM classification method to partition changes in mean and extreme precipitation caused by LUC to thermodynamic and dynamic changes using

500-hPa GPH and precipitation obtained from WRF simulations of the 2001–2010 period. The YRB is used as an example, two factual use cases and two hypothetical reforestation scenarios were set to evaluate the impact of LUC on precipitation in the YRB. The following conclusions can be drawn.

1. The LUC has impacts on the frequency of the circulation pattern, but these impacts are not significant.
2. The factual process of LUC results in a decrease in summer mean daily precipitation, extreme precipitation totals and occurrences of precipitation extremes for most regions of the YRB. However, extreme precipitation in the middle reaches of the YRB tends to increase due to LUC.
3. Reforestation leads to an increase in summer mean daily precipitation, extreme precipitation totals and occurrences of precipitation extremes in the YRB, but the effects of reforestation on increasing precipitation are limited when the reforestation proportion comes to a certain value.
4. The thermodynamic change is the major contributor to changes in precipitation due to LUC with its contribution ranging from 94 to 102%, while dynamic and combined changes only make a small contribution to changes in precipitation due to LUC.

Even though this study found that changes in precipitation due to LUC are primarily contributed by the thermodynamic effect, the results may be subjected to multiple uncertainties. (1) The 500 hPa GPH was used to identify the different atmospheric patterns, the results may not be same when using other atmospheric variables, even though similar results were obtained when using the sea level pressure. (2) Only the WRF model with one simulation was used to investigate the impacts of LUC, the results may be different when using other models or driving the model multiple times, due to climate model uncertainty and internal climate variability. Therefore, more simulations should be conducted by using other models for running multiple simulations in future studies. (3) All WRF simulations were driven by the same lateral boundary condition derived from the ERA-interim reanalysis. The same lateral boundary condition can suppress the difference between various WRF simulations to a certain extent, especially when the model domain is small. Thus the experimental design may also underestimate the LUC effects. (4) Although the impacts of LUC on seasonal mean daily precipitation, extreme precipitation totals and occurrence frequency of precipitation extremes have been evaluated and linked to changes in thermodynamic and dynamic, it does not make a comprehensive explanation in terms of the physical

mechanism. Therefore, further analyses are needed to thoroughly explain the effects of LUC on the causes of precipitation.

## ACKNOWLEDGEMENTS

This work was partially supported by the National Key Research and Development Program of China (Grant No. 2017YFA0603704), the Hubei Provincial Natural Science Foundation of China (Grant No. 2020CFA100), the National Natural Science Foundation of China (Grant No. 52079093), and the Overseas Expertise Introduction Project for Discipline Innovation (111 Project) funded by Ministry of Education and State Administration of Foreign Experts Affairs P.R. China (Grant No. B18037). The data for this study are available at the National Meteorological Information Center, China Meteorological Administration (<http://cdc.cma.gov.cn/home.do>) and European Centre for Medium-Range Weather Forecasts (<http://apps.ecmwf.int/datasets/>). The numerical calculations in this article have been done on the supercomputing system in the Supercomputing Center of Wuhan University.

## ORCID

*Qian Lin*  <https://orcid.org/0000-0003-0058-1223>

*Jie Chen*  <https://orcid.org/0000-0001-8260-3160>

## REFERENCES

- Cassano, E.N., Lynch, A.H., Cassano, J.J. and Koslow, M.R. (2006a) Classification of synoptic patterns in the western Arctic associated with extreme events at Barrow, Alaska, USA. *Climate Research*, 30(2), 83–97. <https://doi.org/10.3354/cr030083>.
- Cassano, J.J., Uotila, P. and Lynch, A. (2006b) Changes in synoptic weather patterns in the polar regions in the twentieth and twenty-first centuries, part 1: Arctic. *International Journal of Climatology*, 26(8), 1027–1049. <https://doi.org/10.1002/joc.1306>.
- Cassano, J.J., Uotila, P., Lynch, A.H. and Cassano, E.N. (2007) Predicted changes in synoptic forcing of net precipitation in large Arctic river basins during the 21st century. *Journal of Geophysical Research-Biogeosciences*, 112(G4), G04S49. <https://doi.org/10.1029/2006jg000332>.
- Chang, C.P., Zhang, Y.S. and Li, T. (2000) Interannual and interdecadal variations of the East Asian summer monsoon and tropical Pacific SSTs. Part I: Roles of the subtropical ridge. *Journal of Climate*, 13(24), 4310–4325. [https://doi.org/10.1175/1520-0442\(2000\)013<4310:iaivot>2.0.co;2](https://doi.org/10.1175/1520-0442(2000)013<4310:iaivot>2.0.co;2).
- Charney, J., Stone, P.H. and Quirk, W.J. (1975) Drought in the sahara: a biogeophysical feedback mechanism. *Science*, 187 (4175), 434–435.
- Chen, Y.R., Li, Y.Q. and Kang, L. (2019) An index reflecting meso-scale vortex-vortex interaction and its diagnostic applications for rainstorm area. *Atmospheric Science Letters*, 20(6), 10. <https://doi.org/10.1002/asl.902>.
- Coumou, D., Petoukhov, V., Rahmstorf, S., Petri, S. and Schellnhuber, H.J. (2014) Quasi-resonant circulation regimes and hemispheric synchronization of extreme weather in boreal

- summer. *Proceedings of the National Academy of Sciences of the United States of America*, 111(34), 12331–12336. <https://doi.org/10.1073/pnas.1412797111>.
- Cui, L.F., Wang, L.C., Lai, Z.P., Tian, Q., Liu, W. and Li, J. (2017) Innovative trend analysis of annual and seasonal air temperature and rainfall in the Yangtze River Basin, China during 1960–2015. *Journal of Atmospheric and Solar-Terrestrial Physics*, 164, 48–59. <https://doi.org/10.1016/j.jastp.2017.08.001>.
- Dee, D.P., Uppala, S.M., Simmons, A.J., Berrisford, P., Poli, P., Kobayashi, S. and Vitart, F. (2011) The ERA-Interim reanalysis: configuration and performance of the data assimilation system. *Quarterly Journal of the Royal Meteorological Society*, 137(656), 553–597. <https://doi.org/10.1002/qj.828>.
- Demuzere, M., Oleson, K., Coutts, A.M., Pigeon, G. and van Lipzig, N.P.M. (2013) Simulating the surface energy balance over two contrasting urban environments using the Community Land Model Urban. *International Journal of Climatology*, 33(15), 3182–3205. <https://doi.org/10.1002/joc.3656>.
- Dewan, A.M., Yamaguchi, Y. and Ziaur Rahman, M. (2012) Dynamics of land use/cover changes and the analysis of landscape fragmentation in Dhaka Metropolitan, Bangladesh. *GeoJournal*, 77 (3), 315–330. <https://doi.org/10.1007/s10708-010-9399-x>.
- Efron, B. and Tibshirani, R.J. (1993) *An Introduction to the Bootstrap*. New York: Chapman and Hall.
- Emori, S. and Brown, S.J. (2005) Dynamic and thermodynamic changes in mean and extreme precipitation under changed climate. *Geophysical Research Letters*, 32(17), 5. <https://doi.org/10.1029/2005gl023272>.
- Fu, B.J., Wang, S., Liu, Y., Liu, J.B., Liang, W. and Miao, C.Y. (2017) Hydrogeomorphic ecosystem responses to natural and anthropogenic changes in the loess plateau of China. *Annual Review of Earth and Planetary Sciences*, 45, 223–243.
- Gascoigne, W.R., Hoag, D., Koontz, L., Tangen, B.A., Shaffer, T.L. and Gleason, R.A. (2011) Valuing ecosystem and economic services across land-use scenarios in the Prairie Pothole Region of the Dakotas, USA. *Ecological Economics*, 70(10), 1715–1725. <https://doi.org/10.1016/j.ecolecon.2011.04.010>.
- Geneletti, D. (2013) Assessing the impact of alternative land-use zoning policies on future ecosystem services. *Environmental Impact Assessment Review*, 40, 25–35. <https://doi.org/10.1016/j.eiar.2012.12.003>.
- Grawe, D., Thompson, H.L., Salmond, J.A., Cai, X.M. and Schlunzen, K.H. (2013) Modelling the impact of urbanisation on regional climate in the Greater London Area. *International Journal of Climatology*, 33(10), 2388–2401. <https://doi.org/10.1002/joc.3589>.
- Grell, G.A. and Devenyi, D. (2002) A generalized approach to parameterizing convection combining ensemble and data assimilation techniques. *Geophysical Research Letters*, 29(14), 38-1–38-4. <https://doi.org/10.1029/2002gl015311>.
- Gui, Z., Zheng, Y., Zeng, X. and Qiang, X. (2014) Impact of different planetary boundary layer parameterizations on summer monsoonal climate simulation in East Asia. *Journal of the Meteorological Sciences*, 34(6), 638–646 (in Chinese).
- Guo, J.L., Guo, S.L., Li, Y., Chen, H. and Li, T.Y. (2013) Spatial and temporal variation of extreme precipitation indices in the Yangtze River basin, China. *Stochastic Environmental Research and Risk Assessment*, 27(2), 459–475. <https://doi.org/10.1007/s00477-012-0643-4>.
- Hewitson, B.C. and Crane, R.G. (2002) Self-organizing maps: applications to synoptic climatology. *Climate Research*, 22(1), 13–26. <https://doi.org/10.3354/cr022013>.
- Hong, S.Y., Noh, Y. and Dudhia, J. (2006) A new vertical diffusion package with an explicit treatment of entrainment processes. *Monthly Weather Review*, 134(9), 2318–2341. <https://doi.org/10.1175/mwr3199.1>.
- Horton, D.E., Johnson, N.C., Singh, D., Swain, D.L., Rajaratnam, B. and Diffenbaugh, N.S. (2015) Contribution of changes in atmospheric circulation patterns to extreme temperature trends. *Nature*, 522(7557), 465–469. <https://doi.org/10.1038/nature14550>.
- Hu, Y., Zhang, X.Z., Mao, R., Gong, D.Y., Liu, H.B. and Yang, J. (2015) Modeled responses of summer climate to realistic land use/cover changes from the 1980s to the 2000s over eastern China. *Journal of Geophysical Research-Atmospheres*, 120(1), 167–179. <https://doi.org/10.1002/2014jd022288>.
- Huang, D.L. and Gao, S.B. (2017) Impact of different cumulus convective parameterization schemes on the simulation of precipitation over China. *Tellus Series A-Dynamic Meteorology and Oceanography*, 69, 13. <https://doi.org/10.1080/16000870.2017.1406264>.
- Huang, H., Jiang, Z., Wang, Z. and Chen, W. (2015) The evaluation of the 500 hPa geopotential height's main modes in East Asia as done by the CMIP5 models. *Acta Meteorologica Sinica*, 73(1), 110–127 (in Chinese).
- Huang, R.H., Chen, D. and Liu, Y. (2012) Characteristics and causes of the occurrence of flooding disaster and persistent heavy Raifnall in the Yangtze River valley of China. *Journal of Chengdu University of Information Technology*, 27(01), 1–19 (in Chinese).
- Jezequel, A., Cattiaux, J., Naveau, P., Radanovics, S., Ribes, A., Vautard, R. and Yiou, P. (2018) Trends of atmospheric circulation during singular hot days in Europe. *Environmental Research Letters*, 13(5), 054007. <https://doi.org/10.1088/1748-9326/aab5da>.
- Kohonen, T. (1998) The self-organizing map. *Neurocomputing*, 21 (1–3), 1–6. [https://doi.org/10.1016/s0925-2312\(98\)00030-7](https://doi.org/10.1016/s0925-2312(98)00030-7).
- Kong, L.Q., Zheng, H., Rao, E.M., Xiao, Y., Ouyang, Z.Y. and Li, C. (2018) Evaluating indirect and direct effects of eco-restoration policy on soil conservation service in Yangtze River Basin. *Science of the Total Environment*, 631–632, 887–894. <https://doi.org/10.1016/j.scitotenv.2018.03.117>.
- Lee, S. and Feldstein, S.B. (2013) Detecting ozone- and greenhouse gas-driven wind trends with observational data. *Science*, 339 (6119), 563–567. <https://doi.org/10.1126/science.1225154>.
- Li, Y., Piao, S.L., Li, L.Z.X., Chen, A.P., Wang, X.H., Ciais, P. and Zhou, L.M. (2018) Divergent hydrological response to large-scale afforestation and vegetation greening in China. *Science Advances*, 4(5), 9. <https://doi.org/10.1126/sciadv.aar4182>.
- Li, Y., Zhou, W.C., Chen, X.Y., Fang, D.X. and Zhang, Q.Q. (2017) Influences of the Three Gorges Dam in China on Precipitation over Surrounding Regions. *Journal of Meteorological Research*, 31(4), 767–773. <https://doi.org/10.1007/s13351-017-6177-4>.
- Lin, Y.L., Farley, R.D. and Orville, H.D. (1983) Bulk parameterization of the snow field in a cloud model. *Journal of Climate and Applied Meteorology*, 22(6), 1065–1092. [https://doi.org/10.1175/1520-0450\(1983\)022<1065:bpotsf>2.0.co;2](https://doi.org/10.1175/1520-0450(1983)022<1065:bpotsf>2.0.co;2).
- Liu, J.Y., Zhang, Z.X., Zhuang, D.F., Wang, Y.M., Zhou, W.C., Zhang, S.W., Li, R.D., J, N. & Wu, S.X. (2003b) A study on the

- spatial temporal dynamic changes of land use and driving forces analyses of China in the 1990s. *Geographical Research*, 22(1), 1–12 (in Chinese).
- Liu, J.G., Daily, G.C., Ehrlich, P.R. and Luck, G.W. (2003a) Effects of household dynamics on resource consumption and biodiversity. *Nature*, 421(6922), 530–533. <https://doi.org/10.1038/nature01359>.
- Liu, Y. and Weisberg, R.H. (2011) In: Mwasiagi, J.I. (Ed.) *A Review of Self-Organizing Map Applications in Meteorology and Oceanography, Self Organizing Maps—Applications and Novel Algorithm Design*. Croatia: InTech. 253–272.
- Liu, Z.J. and Liu, Y.S. (2018) Does anthropogenic land use change play a role in changes of precipitation frequency and intensity over the loess plateau of China? *Remote Sensing*, 10(11), 14. <https://doi.org/10.3390/rs10111818>.
- Michaelides, S., Pattichis, C.S. and Kleovoulou, G. (2001) Classification of rainfall variability by using artificial neural networks. *International Journal of Climatology*, 21(11), 1401–1414. <https://doi.org/10.1002/joc.702>.
- Mioduszewski, J.R., Rennermalm, A.K., Hammann, A., Tedesco, M., Noble, E.U., Stroeve, J.C. and Mote, T.L. (2016) Atmospheric drivers of Greenland surface melt revealed by self-organizing maps. *Journal of Geophysical Research-Atmospheres*, 121(10), 5095–5114. <https://doi.org/10.1002/2015jd024550>.
- Niu, G.Y., Yang, Z.L., Mitchell, K.E., Chen, F., Ek, M.B., Barlage, M. and Xia, Y.L. (2011) The community Noah land surface model with multiparameterization options (Noah-MP): 1. Model description and evaluation with local-scale measurements. *Journal of Geophysical Research-Atmospheres*, 116, 19. <https://doi.org/10.1029/2010jd015139>.
- Otterman, J. (1974) Baring high-albedo soils by overgrazing: a hypothesized desertification mechanism. *Science*, 186(4163), 531–533.
- Reusch, D.B. (2010) Nonlinear climatology and paleoclimatology: capturing patterns of variability and change with self-organizing maps. *Physics and Chemistry of the Earth*, 35(9–12), 329–340. <https://doi.org/10.1016/j.pce.2009.09.001>.
- Reusch, D.B., Alley, R.B. and Hewitson, B.C. (2005) Relative performance of self-organizing maps and principal component analysis in pattern extraction from synthetic climatological data. *Polar Geography*, 29(3), 188–212.
- Sagan, C., Toon, O.B. and Pollack, J.B. (1979) Anthropogenic albedo changes and the Earth's climate. *Science*, 206(4425), 1363–1368.
- Sang, Y.F., Wang, Z.G. and Liu, C.M. (2013) Spatial and temporal variability of daily temperature during 1961–2010 in the Yangtze River Basin, China. *Quaternary International*, 304, 33–42. <https://doi.org/10.1016/j.quaint.2012.05.026>.
- Seager, R., Naik, N. and Vecchi, G.A. (2010) Thermodynamic and dynamic mechanisms for large-scale changes in the hydrological cycle in response to global warming. *Journal of Climate*, 23 (17), 4651–4668. <https://doi.org/10.1175/2010jcli3655.1>.
- Shu, L., Wang, T.J., Han, H., Xie, M., Chen, P.L., Li, M.M. and Wu, H. (2020) Summertime ozone pollution in the Yangtze River Delta of eastern China during 2013–2017: synoptic impacts and source apportionment. *Environmental Pollution*, 257, 11. <https://doi.org/10.1016/j.envpol.2019.113631>.
- Skamarock, W.C., Klemp, J.B., Dudhia, J., Gill, D.O., Barker, D.M., Duda, M.G., Huang, X.Y., Wang, W. and Powers, J.G. (2008) *A description of the advanced research WRF version 3*. NCAR Technical Note NCAR/TN-475+STR, 125 pp., National Center for Atmospheric Research, Boulder, CO.
- Skific, N., Francis, J.A. and Cassano, J.J. (2009) Attribution of projected changes in atmospheric moisture transport in the Arctic: a self-organizing map perspective. *Journal of Climate*, 22(15), 4135–4153. <https://doi.org/10.1175/2009jcli2645.1>.
- Sterling, S.M., Ducharme, A. and Polcher, J. (2013) The impact of global land-cover change on the terrestrial water cycle. *Nature Climate Change*, 3(4), 385–390. <https://doi.org/10.1038/nclimate1690>.
- Su, B.D., Jiang, T. and Jin, W.B. (2006) Recent trends in observed temperature and precipitation extremes in the Yangtze River basin, China. *Theoretical and Applied Climatology*, 83(1–4), 139–151. <https://doi.org/10.1007/s00704-005-0139-y>.
- Tan, X.Z., Gan, T.Y., Chen, S., Horton, D.E., Chen, X.H., Liu, B.J. and Lin, K.R. (2019) Trends in persistent seasonal-scale atmospheric circulation patterns responsible for seasonal precipitation totals and occurrences of precipitation extremes over Canada. *Journal of Climate*, 32(21), 7105–7126. <https://doi.org/10.1175/jcli-d-18-0408.1>.
- Wang, H.C. and Zhong, Z. (2014) Ensemble simulations to investigate the impact of large-scale urbanization on precipitation in the lower reaches of Yangtze River Valley, China. *Quarterly Journal of the Royal Meteorological Society*, 140(678), 258–266. <https://doi.org/10.1002/qj.2125>.
- Wang, K., Zhang, Q., Chen, Y.D. and Singh, V.P. (2015) Effects of land-use/cover change on hydrological processes using a GIS-RS-based integrated hydrological model: case study of the East River, China. *Hydrological Sciences Journal*, 60(10), 1724–1738. <https://doi.org/10.1080/02626667.2014.949723>.
- Wang, W.J., Guo, H.C., Chuai, X.W., Dai, C., Lai, L. and Zhang, M. (2014) The impact of land use change on the temporospatial variations of ecosystems services value in China and an optimized land use solution. *Environmental Science & Policy*, 44, 62–72. <https://doi.org/10.1016/j.envsci.2014.07.004>.
- Wang, Y. and Yan, Z.W. (2011) Changes of frequency of summer precipitation extremes over the Yangtze River in association with large-scale oceanic-atmospheric conditions. *Advances in Atmospheric Sciences*, 28(5), 1118–1128. <https://doi.org/10.1007/s00376-010-0128-7>.
- Wei, J.F., Dirmeyer, P.A., Bosilovich, M.G. and Wu, R.G. (2012) Water vapor sources for Yangtze River Valley rainfall: climatology, variability, and implications for rainfall forecasting. *Journal of Geophysical Research-Atmospheres*, 117, D05126. <https://doi.org/10.1029/2011jd016902>.
- Wilks, D.S. (2006) On "field significance" and the false discovery rate. *Journal of Applied Meteorology and Climatology*, 45(9), 1181–1189. <https://doi.org/10.1175/jam2404.1>.
- Wu, L.G., Zhang, Q. and Jiang, Z.H. (2006) Three Gorges Dam affects regional precipitation. *Geophysical Research Letters*, 33 (13), 4. <https://doi.org/10.1029/2006gl026780>.
- Xu, M. and Ma, C. (2009) *Yangtze River Basin Climate Change Vulnerability and Adaptation Report*. Beijing: China Water Power Press.
- Yang, H. and Sun, S.Q. (2005) The characteristics of longitudinal movement of the subtropical high in the western Pacific in the pre-rainy season in South China. *Advances in Atmospheric Sciences*, 22(3), 392–400.
- Yang, Z.L., Niu, G.Y., Mitchell, K.E., Chen, F., Ek, M.B., Barlage, M. and Xia, Y.L. (2011) The community Noah land surface model

- with multiparameterization options (Noah-MP): 2. Evaluation over global river basins. *Journal of Geophysical Research-Atmospheres*, 116, 16. <https://doi.org/10.1029/2010jd015140>.
- Yin, J., Wang, D. and Zhai, G. (2014) A study of characteristics of the cloud microphysical parameterization schemes in meso-scale models and its applicability to China. *Advance in Earth Sciences*, 29(2), 238–249 (in Chinese).
- Yu, E.T., Wang, H.J., Gao, Y.Q. and Sun, J.Q. (2011) Impacts of cumulus convective parameterization schemes on summer monsoon precipitation simulation over China. *Acta Meteorologica Sinica*, 25 (5), 581–592. <https://doi.org/10.1007/s13351-011-0504-y>.
- Yu, F.L., Chen, Z.Y., Ren, X.Y. and Yang, G.F. (2009) Analysis of historical floods on the Yangtze River, China: characteristics and explanations. *Geomorphology*, 113(3–4), 210–216. <https://doi.org/10.1016/j.geomorph.2009.03.008>.
- Zhang, C.L., Chen, F., Miao, S.G., Li, Q.C., Xia, X.A. and Xuan, C. Y. (2009) Impacts of urban expansion and future green planting on summer precipitation in the Beijing metropolitan area. *Journal of Geophysical Research-Atmospheres*, 114, D02116. <https://doi.org/10.1029/2008jd010328>.
- Zhang, G.H., Ding, W.F., Wang, Y.F. and Xiao, H. (2020) Analysis on water and sediment variation and the driving factors in Yangtze River Basin since 2000. *Journal of Soil and Water Conservation*, 34(3), 98–104+206.
- Zhang, H., Wu, C.H., Chen, W.J. and Huang, G.R. (2019) Effect of urban expansion on summer rainfall in the Pearl River Delta, South China. *Journal of Hydrology*, 568, 747–757. <https://doi.org/10.1016/j.jhydrol.2018.11.036>.
- Zhang, N., Gao, Z.Q., Wang, X.M. and Chen, Y. (2010) Modeling the impact of urbanization on the local and regional climate in Yangtze River Delta, China. *Theoretical and Applied Climatology*, 102 (3–4), 331–342. <https://doi.org/10.1007/s00704-010-0263-1>.
- Zhang, Q. and Tao, S. (1998) Influence of Asian mid-high latitude circulation on East Asian summer rainfall. *Acta Meteorologica Sinica*, 56(2), 199–211.
- Zhao, G.J., Hoermann, G., Fohrer, N., Gao, J.F., Zhai, J.Q. and Zhang, Z.X. (2009) Spatial and temporal characteristics of wet spells in the Yangtze River Basin from 1961 to 2003. *Theoretical and Applied Climatology*, 98(1–2), 107–117. <https://doi.org/10.1007/s00704-008-0099-0>.
- Zhi, X.F. and Ji, L.Y. (2018) BMA probabilistic forecasting of the 500hPa Geopotential height over northern hemisphere using TIGGE multimodel ensemble forecasts. In: Bardis, N. (Ed.) *Mathematical Methods and Computational Techniques in Science and Engineering II*, Vol. 1982. Melville: American Institute of Physics.
- Zwiers, F.W. and von Storch, H. (1995) Taking serial correlation into account in tests of the mean. *Journal of Climate*, 8(2), 336–351.

## SUPPORTING INFORMATION

Additional supporting information may be found online in the Supporting Information section at the end of this article.

**How to cite this article:** Lin Q, Chen J, Li W, Huang K, Tan X, Chen H. Impacts of land use change on thermodynamic and dynamic changes of precipitation for the Yangtze River Basin, China. *Int J Climatol*. 2021;41:3598–3614. <https://doi.org/10.1002/joc.7037>